Open Access

Changes on Texture and Crystalline Phase of Activated Carbon-Supported Ni-Ca Catalyst During Dry Methane Reforming

Juan Matos[*,1], Maibelin Rosales[1], Gema González[1] and Caribay Urbina de Navarro[2]

[1]*Engineering of Materials and Nanotechnology Centre, Venezuelan Institute for Scientific Research, I.V.I.C., 20632, Caracas 1020-A, Venezuela*

[2]*Centre for Electron Microscopy, Central University of Venezuela, Caracas 1040, Venezuela*

Abstract: Changes on texture and crystalline phase of AC-supported Ni-Ca catalyst during dry methane reforming were verified. Characterization by N_2 adsorption, XPS, XRD, TEM and HR-TEM was performed. XPS and XRD analysis suggest that the initial activity can be attributed to a nickel reduced phase formed during helium pre-treatment. TEM showed that a homogeneous distribution of Ni nanoparticles between 10-20nm at the tip of multi-walled carbon nanotubes is formed during reaction. HR-TEM showed diffusion of Ni nanoparticles and the formation of carbon-like nano onions with an interlayer separation of 0.5nm suggesting the formation of a ultra-microporous carbon structure. An increase in surface area from 231$m^2.g^{-1}$ to 2405$m^2.g^{-1}$ after 90min reaction was found and attributed to an *in situ* activation of carbon deposits by CO_2 gasification. The present results suggest that introducing CO_2 pulses during reaction carbon-supported Ni-Ca could be employed as potential catalysts for methane and other hydrocarbon reforming reactions at mild experimental conditions.

Keywords: Activation, Carbon deposits, Dry methane reforming, Ni-based catalyst.

1. INTRODUCTION

In the following years is expected an increasing production and conversion of methane because it is the main component of natural gas. Methane can be transformed to syngas by reforming and this mixture of CO and H_2 can be employed to obtain different upgrading molecules as green diesel, methanol and dimethyl ether. Though the supported noble metals catalysts showed the highest activity for methane conversion reactions [1-3] an economic alternative are nickel-based catalysts [4-7]. The industrial development of Ni-based catalysts in dry methane reforming is not well established due to its poor stability, mainly by high coking rates and consequent deactivation phenomena [2,4]. In addition, activity and stability of Ni-based catalysts for methane conversion reactions depend on texture and surface properties of supports [6,7]. Activated carbon (AC) presents several advantages such as low cost, control of texture and surface chemistry during synthesis, high thermal conductivity, easy recovery of active phase from deactivated catalysts and so on [8,9] to be employed as catalytic support. However, activated carbon is not a common catalytic support for methane reforming reactions [10] because it can suffer gasification by steam or by CO_2. Both reactions are spontaneous at about 700ºC but in a preliminary study of dry methane reforming on a carbon-supported Ni-Ca catalyst [11] we showed CO_2 can help control excess of carbon deposits without any detrimental effect on carbon supports after 5h reaction at 650ºC. It was also reported [11] that NiCa/AC catalyst pre-treated under helium flow at temperatures from 550 up to 800ºC showed higher methane conversions than those obtained after pre-treatment under H_2 flow. However, contrary to our preliminary work [11], Chen and co-workers [7] reported that in absence of carbon dioxide or steam an activated carbon-supported nickel-based catalyst was deactivated by Ni_3C formed during methane decomposition. Li and co-workers [12] found that the catalytic activity of pure Ni catalyst for methane decomposition was related to the crystalline size of reduced Ni. They pointed out that during reaction Ni particles suffered important changes. They suggested that carbon deposits in the shape of carbon nanofilaments affect both size and morphology of metallic nickel crystals and these same authors [13] found that the diameter of carbon filaments is controlled by the size of catalyst particles. The objective of this work is to study the changes on texture and crystalline phase of AC-supported Ni-Ca catalyst during dry methane reforming at mild experimental conditions and to correlate these changes with activity and stability of catalyst.

2. EXPERIMENTAL

Ni(5wt%)-Ca(1wt%) catalyst was prepared by incipient wetness impregnation with nickel and calcium nitrate solutions on a commercial activated carbon (AC) purchased from Merck [Langmuir surface area 907m^2g^{-1}, 22Å mean pore width, ash content <1wt%] following the procedure described in previous works [10,11]. Impregnation order is given by the sequence of elements, i.e., Ni followed by Ca. This catalyst was chosen because in a previous study [10] it showed the best activity for dry methane reforming. Characterization by N_2 adsorption-desorption isotherms, X-ray photoelectron spectroscopy (XPS), X-ray diffraction (XRD) and transmission electron microscopy (TEM, HR-

*Address correspondence to this author at the Engineering of Materials and Nanotechnology Centre, Venezuelan Institute for Scientific Research, I.V.I.C., 20632, Caracas 1020-A, Venezuela; Tel/Fax: +58-212-5041922; E-mail: jmatos@ivic.gob.ve

1874-088X/10 2010 Bentham Open

TEM) was performed. N_2 adsorption-desorption isotherms permit to verify the changes in textural properties of the catalysts. XPS spectra permit to verify mainly the change in electronic states of nickel and its interaction with carbon support. XRD patterns permit to verify the changes in crystalline phases of nickel species and the presence of metallic carbides crystallites. TEM studies permit to verify the changes in morphology and topology of the catalyst. *Ex-situ* XPS was carried out in an ESCALAB 220i-XL spectrometer (VG Scientific) equipped with a hemispherical electron analyzer and a double anode Mg-Al non-monochromatic X-ray source. The pressure in the analysis chamber was kept below 10^{-9}Torr. Samples were protected from exposition to the atmosphere by immersion into an ultra-dry hydrocarbon solvent (purified heptanes) while transferring from the reactor to the chamber of the spectrometer. Texture characterization was performed by N_2 adsorption-desorption isotherms at 77K. The full isotherms in the range of $4x10^{-3}$ to 84 kPa were measured in a Micromeritics ASAP-2010. Surface area, micropore area, pore volume and pore diameters were obtained by Langmuir isotherms, t-plot method and Harkins-Jura [14] method, respectively. These methods were employed because they permit an accounting for the adsorbed layer on pore walls, when calculating pore size distribution, and they are very useful when different types of pores are involved. Langmuir isotherm and Harkins-Jura method are appropriate for the present case because samples contain slits and spherical pores. Powder X-ray diffraction (XRD) patterns were recorded in the range of 2θ = 10-80º on a D-5005 diffractometer from Siemens with Cu Kα (1.54056) radiation and processed with the Diffrac-Plus-Eva program. A transmission electron microscope (TEM) operating at 100keV accelerating voltage was used for the microscopy study. TEM samples were prepared from ethanol suspensions and placed on copper grids. HR-TEM was performed in a TECNAI ST G-20 equipment operating at 200keV. Catalyst´s samples were *in situ* pre-treated under helium flow ($50cm^3.min^{-1}$, 100kPa pressure) at 650ºC with a heating rate of 10ºC/min before reaction. Catalytic activity was followed in a continuous flow system (quartz reactor) flowing both reactants (CH_4 and CO_2) at nearly atmospheric pressure (100kPa). Analysis of CH_4 was carried out with gas chromatography (Varian 3700 GC apparatus) with a flame ionization detector (FID) and employing a Porapak R packed column at 50ºC. Catalytic activity was reported as mmols methane converted by time and catalysts weight. Reaction conditions were the following: 150mg catalyst sample, $80cm^3.min^{-1}$ flow of CH_4 and CO_2 (50vol% each reactant), and reaction temperature 650ºC (similar to that of the pre-treatment). Activity tests were done in triplicate and the reproducibility was better than 5%.

3. RESULTS AND DISCUSSION

3.1. Methane Conversion and XPS Analysis

Fig. (**1**) shows the catalytic activity of Ni/AC and Ni-Ca/AC. Initial activities are very similar with 11.7 and $10.3mmols.min^{-1}.g_{cat}^{-1}$ for Ni/AC (Fig. **1A**) and Ni-Ca/AC (Fig. **1B**), respectively. Activities decreased to 4.2 and $7.7mmols.min^{-1}.g_{cat}^{-1}$ after 4h reaction and to 1.2 and $3.2mmols.min^{-1}.g_{cat}^{-1}$ after 24h reaction. This is a deactivation of 90% and 70% relative to initial activities for Ni/AC and Ni-Ca/AC, respectively. In a previous work [10], we showed that catalytic activity of Ca/AC is negligible [10]. Therefore the present results suggest that calcium, in the form of CaO or $CaCO_3$ [10], would play a promoter role in the present bimetallic system, as has been earlier reported [3,6].

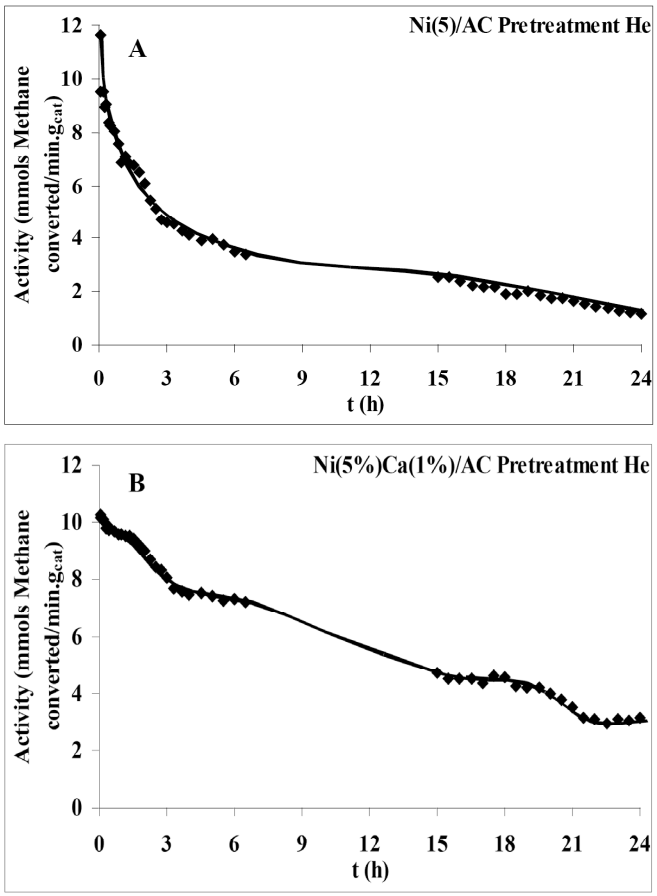

Fig. (1). Catalytic activity after He pretreatment at 650ºC by 1h. (**A**): Ni/AC. (**B**): Ni-Ca/AC.

Activity of Ni-based catalysts can be explained from changes in Ni^{+2} binding energies detected in Ni 2p region from XPS. It can be seen from Fig. (**2**) that in comparison to the crude catalyst the binding energy of nickel in Ni-Ca/AC decreased about 2 eV (from 855.8 eV to 853.9 eV) after He pre-treatment. By contrast, we showed [10] that in absence of calcium, the binding energy of Ni^{+2}, for Ni/AC, only decreased in about 0.9eV after He pre-treatment. The role of electron donors of CaO and $CaCO_3$ is well-known [15] and the present result suggest that calcium phases would induce an easier reduction of Ni^{+2} to lower oxidation states, probably by its interaction with carbon atoms from support [8]. However, the peak found for the binding energy of nickel (853.9 eV) in Ni-Ca/AC catalyst after He pretreatment does not correspond to a full reduction to elemental nickel since the binding energy of Ni^0 is about 852eV. It can be inferred from XPS results (Fig. **2**), that a Ni phase richer in electron density was formed during pre-treatment, probably a mixture of elemental nickel and nickel carbide phases, in the form of NiC or Ni_3C. These metallic carbide phases can be deduced from XPS spectra of C1s region (Fig. **3**). Fig. (**3A**, **B**) present the Gaussian analysis of carbon main peak after He pre-treatment at 650ºC by 1h and after 90min reaction,

respectively. After helium pretreatment, besides a signal about 286.4eV attributed to cyclic ether groups (-C-O-C-) on the surface of activated carbons [11], another signal about 283.9eV was also detected (Fig. **3A**). This signal has been attributed by Mirodatos and co-workers [16] to a nickel carbide phase Ni_3C. These authors showed that nickel carbide-like layers are formed in the initial period of reaction of dry methane reforming. After 90min reaction (Fig. **3B**) the intensity of this signal increase and another signal is also detected about 282.6eV and attributed to carbon filaments [16]. We propose, in agreement with Mirodatos [16] that a mixture of reduced nickel and Ni_3C are responsible for the initial conversion of methane on Ni-Ca/AC catalyst.

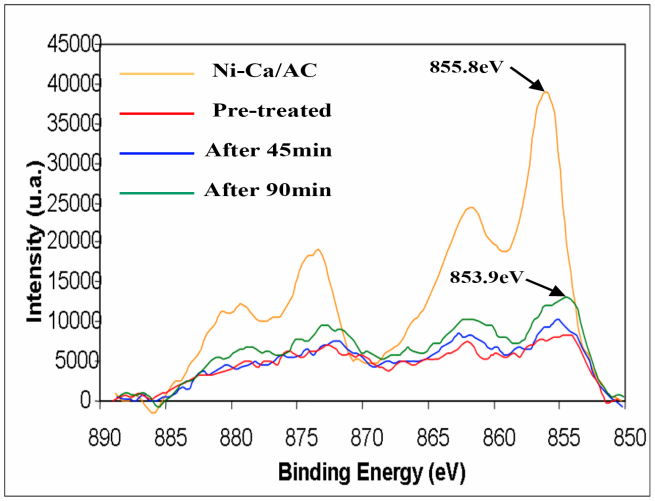

Fig. (2). Changes in XPS spectra in Ni 2p region Ni-Ca/AC catalyst.

3.2. Texture and Crystalline Phase Characterization

N_2 adsorption-desorption isotherms for AC and Ni-Ca/AC catalyst before and after He pretreatment are shown in Fig. (**4**) while Fig. (**5**) shows the N_2 adsorption-desorption isotherms of Ni-Ca/AC catalyst after 45min and 90min reaction. We have chosen these reaction times to characterize the changes in textural properties because in a previous work about ethylene hydrogenation reaction [9] we found that the most important changes on the catalytic activity of Ni-Mo/AC and on nickel crystalline phases occurred during the first 90min reaction. All isotherms in Figs. (**4**, **5**) showed a micro- and mesopores framework and they seem to be an IV-type adsorption isotherms by the hysteresis loop observed. A summary of Langmuir surface area, micropore area, pore volume and mean pore diameters is shown in Table **1**. Ni-Ca/AC catalyst showed an increase in surface area from $231m^2.g^{-1}$ (after pretreatment) up to $2405m^2.g^{-1}$ after 90min reaction. This increase can be attributed to a higher proportion of microporous framework suggested by the enhancement in micropore volume ($0.841cm^3.g^{-1}$ against $0.068cm^3.g^{-1}$). Surface area and micropore volume of Ni-Ca/AC after 90min reaction are clearly higher than those obtained for the AC alone ($2405m^2.g^{-1}$ and $0.841cm^3.g^{-1}$ against $907m^2.g^{-1}$ and $0.268cm^3.g^{-1}$). Therefore, we suggest that carbon deposits formed during reaction clearly affects the global texture of Ni-Ca/AC catalyst. Carbon deposits would be produced primary, from methane disproportion ($CH_4 \rightarrow C + 2H_2$). In addition, since CO is one product

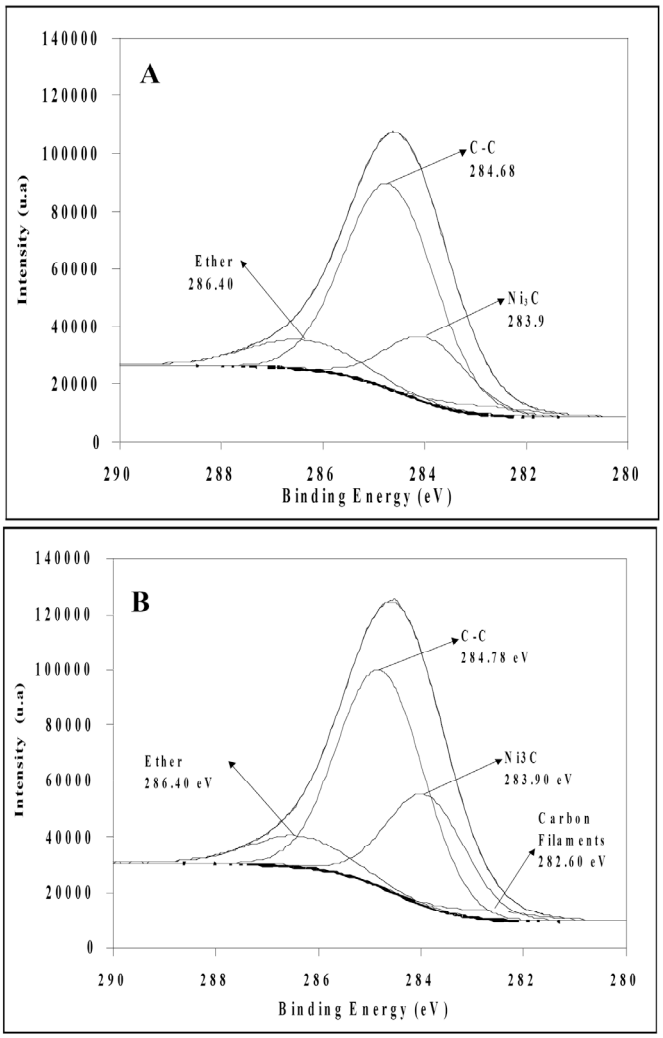

Fig. (3). XPS spectra in C 1s region for Ni-Ca/AC. (**A**): After He pre-treatment at 650ºC, 1h. (**B**): After 90min reaction at 650ºC.

reaction, carbon nanotubes could be formed from carbon monoxide disproportion [17]. However, carbon nanotubes are typical mesoporous materials with a relatively low surface area between $100m^2.g^{-1}$ up to $250m^2.g^{-1}$ [17]. Therefore, is neither possible that an increase in one order magnitude in the surface area in the present work can be due to carbon nanotubes nor to the clean of the internal surface of activated carbon because its surface area is about $907m^2.g^{-1}$ which is clearly lower than $2405\ m^2.g^{-1}$. Therefore, to explain the present results we suggest an *in situ* activation of carbon deposits by gasification with CO_2 according to the reversal Boudouart reaction ($C + CO_2 \rightarrow 2CO$) [18,19]. The overall reaction pathway would involve the adsorption and cracking of methane and CO_2 adsorption to react with carbon deposits as suggested by Xiao *et al.* [20]. The present results are also in agreement with Laine *et al.* [21] whom reported the addition of a micropore framework to a parent Ni-supported activated carbon catalyst by carbon deposits formed from methane and ethylene decomposition.

XRD patterns (Fig. **6**) of Ni-Ca/AC catalyst show the characteristic (012) plane of NiO phase at $2\theta = 43.3°$ in the non pretreated catalyst (Fig. **6A**). This phase is also observed after pre-treatment (Fig. **6B**), after 45min (Fig. **6C**) and

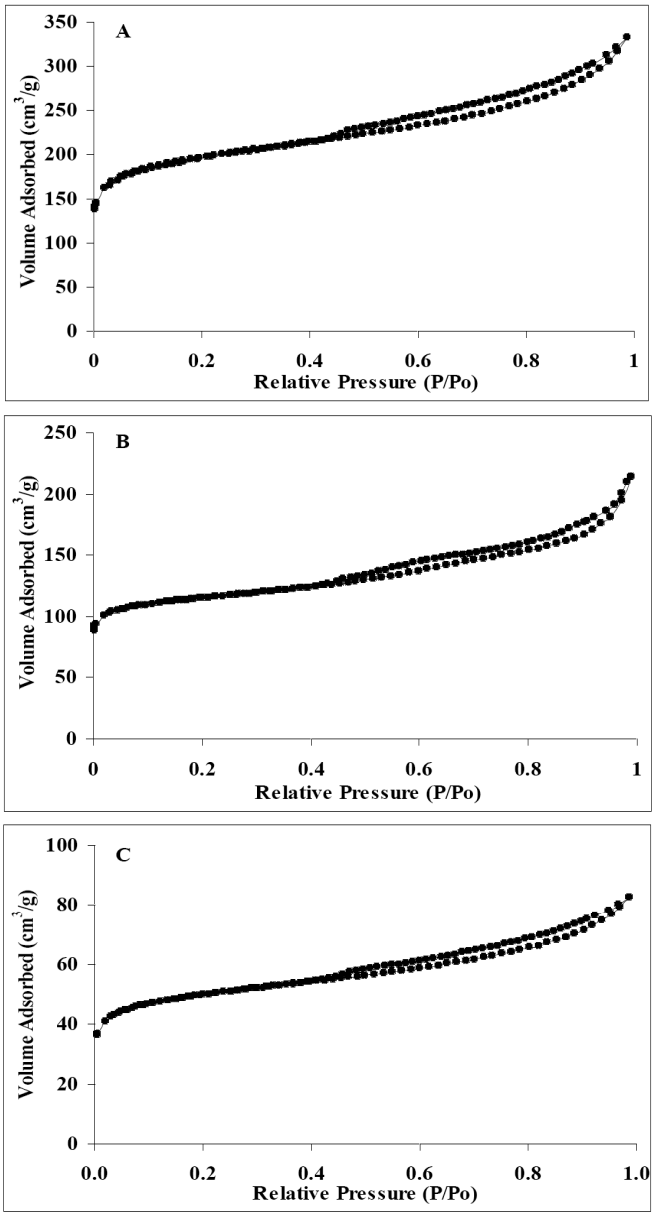

Fig. (4). N_2 adsorption isotherms. (**A**): AC, (**B**): Ni-Ca/AC, (**C**): Ni-Ca/AC after pretreatment under He, 650°C by 1h.

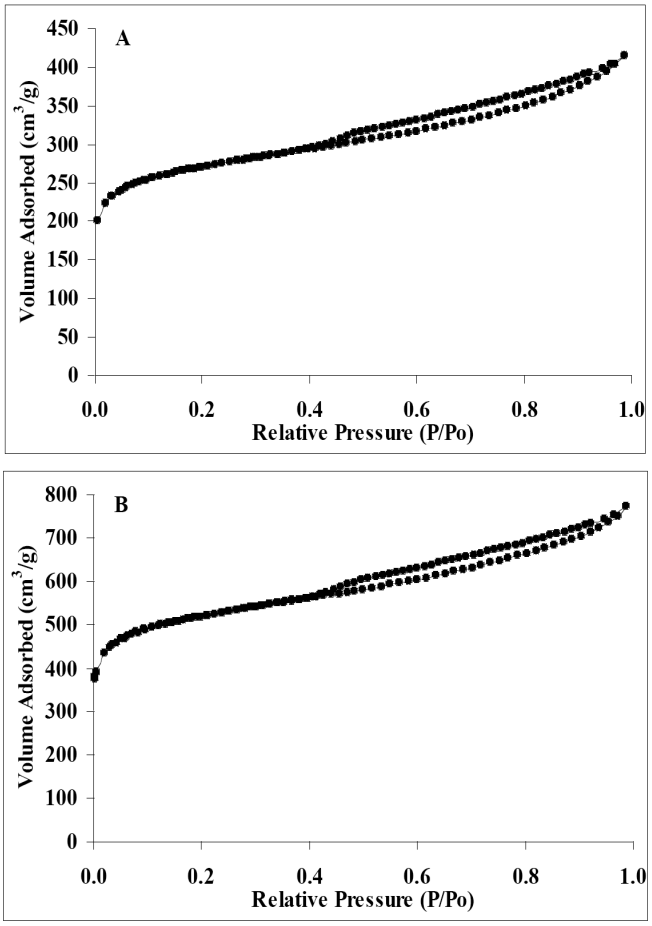

Fig. (5). N_2 adsorption isotherms of Ni-Ca/AC. (**A**): After 45min reaction. (**B**): After 90min reaction.

90min reaction (Fig. **6D**). This peak could overlap the peak of Ni crystallites (111) reported by Li *et al.* [12] but we did not detect a clear reduction in the oxidation state of nickel from Ni^{+2} to Ni^0 (Fig. **2**). However, two new diffraction peaks at 2θ = 52.0º and 2θ = 77.0º can be observed after helium pretreatment (Fig. **6B**). These peaks were attributed to a mixture of Ni crystallites [12] and nickel carbide phases NiC and Ni_3C. The formation of these crystalline phases from the interaction of NiO with activated carbon has been

Table 1. Summary of Textural Properties in AC and Ni-Ca/AC

Textural Properties	AC	Ni-Ca/AC	After He Pretreatment	After 45min Reaction	After 90min Reaction
$S_{Langmuir}$ (m^2/g)	907	529	231	1269	2405
Microporous area (m^2/g)[a]	778	462	200	1134	2219
Microporous proportion (%)[b]	86	86	87	91	92
Total pore volume (cm^3/g)[c]	0.515	0.331	0.128	0.642	1.198
Micropore volume (cm^3/g)[a]	0.268	0.169	0.068	0.426	0.841
Meso/macropore volume (cm^3/g)[d]	0.331	0.211	0.081	0.0381	0.674
Mean pore diameters (Å)[e]	22.7	25.0	22.1	20.2	19.9

[a]Obtained from t-plot method.
[b]Microporous proportion (%) = (microporous area/Langmuir surface area).100.
[c]Pore diameters less than 1489.0816Å at P/P_0 equal to 0.98683317.
[d]For pore diameters between 17Å and 3000Å.
[e]Obtained from Harkins-Jura method [14].

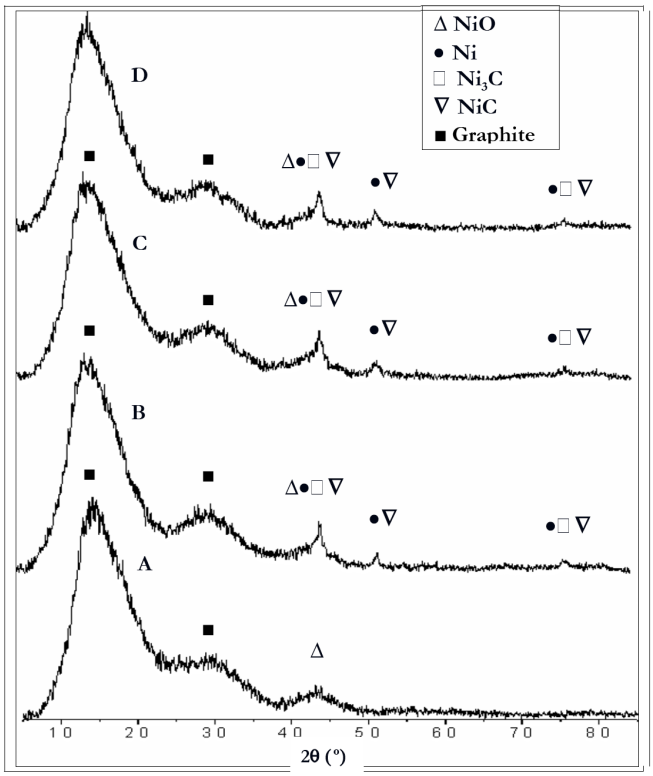

Fig. (6). XRD patterns of Ni-Ca/AC catalyst. (**A**): No treatment. (**B**): After He pre-treatment. (**C**): After 45min reaction. (**D**): After 90min reaction.

already reported by our group [8] in a work related with ethylene hydrogenation on Ni-Mo/AC catalyst. The formation of nickel carbide in the Ni-Ca/AC catalyst can be explained taking into account that Ca atomic radius is larger than that of Ni (2.35 *vs* 1.24Å), then nickel particles would diffuse easier through AC micropore framework to the external surface, and once there these nickel atoms would react with carbon atoms from support or from carbon deposits formed during reaction. This interaction between NiO and C atoms leads to elemental nickel and nickel carbide crystallites, in agreement with results reported by Bai *et al.* [7]. As expected, CaO diffraction peaks were not detected in XRD patterns because the calcium composition in catalyst is only of about 1wt%, and therefore it is diluted by the AC support. A comparison between the percentages in weight of elements constituting Ni-Ca/AC catalyst is compiled in Table **2**. It can be seen that Ni/C atom rate decrease from 0.092 to 0.029 for non-pretreated and pretreated catalyst, respectively and this value remains practically constant after 45 and 90min reaction. These results suggest that the interaction between Ni-catalyst and carbon could occur not only with carbon atoms from support but also from carbon atoms from carbonaceous deposits leading to a dynamic formation of Ni_3C along the reaction. It should be considered that though Ni_3C can be formed at low temperatures it is not thermodynamically stable at high temperatures and therefore it is expected to decompose into C and Ni. A more detailed XRD and *in-situ* XPS studies would be necessary to come to a conclusion of the real influence of Ni_3C phase on catalytic activity of Ni-Ca/AC.

3.3. Carbon Deposits and Morphology

Fig. (**7**) shows a TEM image of Ni-Ca/AC catalyst pre-treated under He flow at 650°C for 1h. A metallic phase with different sizes on AC surface (indicated with black arrows and white circles) can be observed. TEM image from Fig. (**8**) shows a clear change in the morphology of catalyst with the appearance of carbon nanofibers with external diameters of about 30nm. These fibers consist of curved and hollow multi-walled carbon nanotubes (MW-CNT) with an internal diameter around 7-10nm. Also in Fig. (**8**), nanoparticles of different sizes inside and at the CNTs tips were detected. These particles would be mainly composed by different nickel crystallites phases, as discussed above from XPS and XRD studies. Comparison of TEM images in Figs. (**7**, **8**) suggest that crystallites diffused from the external surface of AC (Fig. **7**) along CNT (Fig. **8**). After 90min reaction, TEM image (Fig. **9**) showed that crystallites change into a homogeneous distribution of Ni nanoparticles between 10-20nm sizes. In agreement with the acceptable stability of Ni-Ca/AC catalyst which suffered a decrease in activity of about 70% after 24h reaction relative to the initial activity (Fig. **1**), this highly dispersed Ni nanoparticles distribution would inhibit sintering of catalyst. This distribution could be formed from the fragmentation of nickel particles along the filament growth, with the concomitant formation of smaller crystallites. This fragmentation has been attributed to the appearance of various forces influenced by the specific physical and chemical properties of the support [21,22]. Finally, a HR-TEM study was carried out for the Ni-Ca/AC catalyst after 90min reaction. Nanoparticles (white arrows) with diameters from 5nm (Fig. **10A**) to 10nm (Fig. **10B**) were detected after this reaction time. It should be pointed out the apparent diffusion of crystallites (Fig. **10C**) through several very-well aligned (white arrow) carbon layers. It can be seen from Fig. (**10C**) that about 10 graphene parallel

Table 2. Changes in Atomic Weights (At %) of Elements Detected in Ni-Ca/AC Catalyst from the Corresponding Regions Analyzed by XPS

Sample	Ni	O	Ca	C	Ni/C	Ca/C
AC	- - -	8.505	- - -	91.495	- - -	- - -
Ni-Ca/AC non pre-treated	7.136	14.619	0.407	77.838	0.092	0.0052
Ni-Ca/AC after pre-treatment	2.724	1.528	0.311	95.436	0.029	0.0033
Ni-Ca/AC after 45min reaction	2.261	4.130	0.326	93.264	0.024	0.0035
Ni-Ca/AC after 90min reaction	2.757	5.314	0.330	91.599	0.030	0.0036

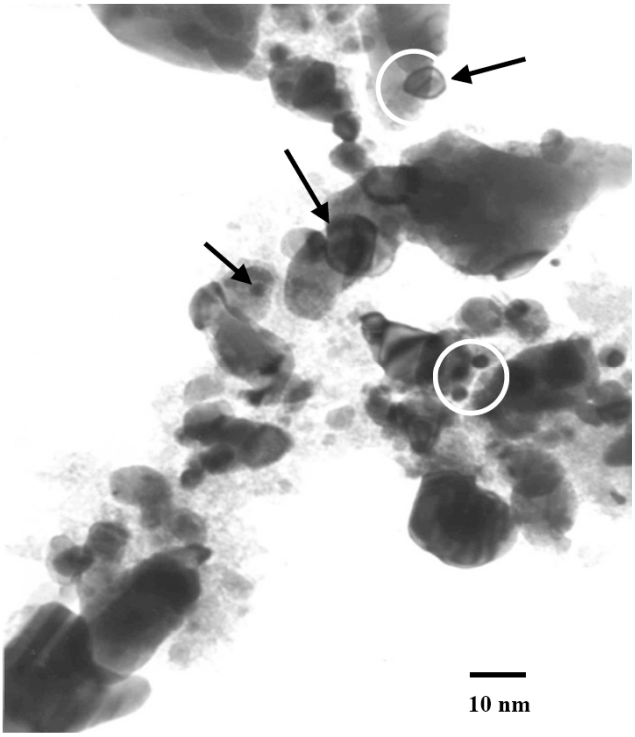

Fig. (7). TEM image of Ni-Ca/AC after He pre-treatment at 650ºC, 1h.

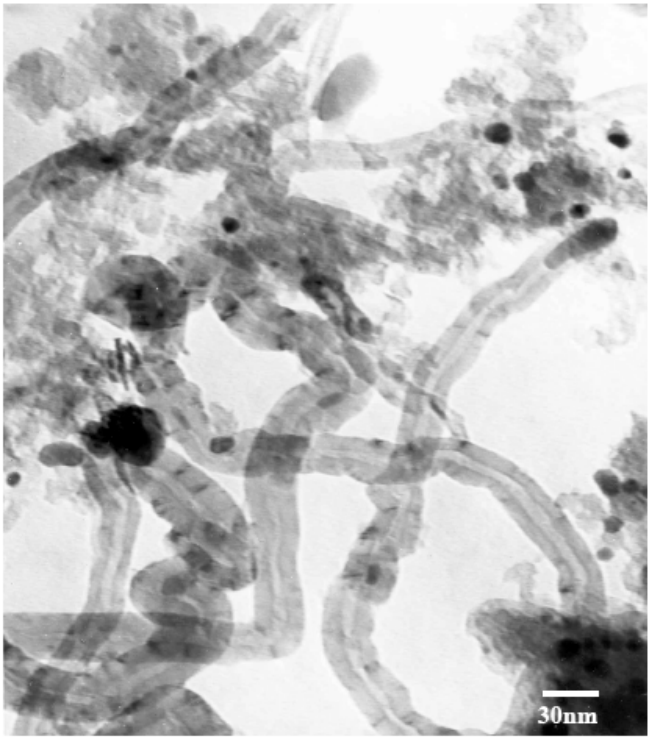

Fig. (8). TEM image of Ni-Ca/AC After 45min reaction at 650ºC.

layers correspond to a separation of 0.5nm/layer. This value is slightly higher than pristine graphite (0.334nm), suggesting that the present carbon deposits would correspond to the specific case of a supermicroporous AC [23,24]. This feature is in fully agreement with the increase in surface area observed in Ni-Ca/AC (Table **1**) that we suggest as the consequence of an *in situ* activation by CO_2 of carbon deposits formed during reaction. In addition, HR-TEM image from Fig. (**10D**) showed that this carbon composite have the apparent morphology of carbon nano onions (white circle) [25].

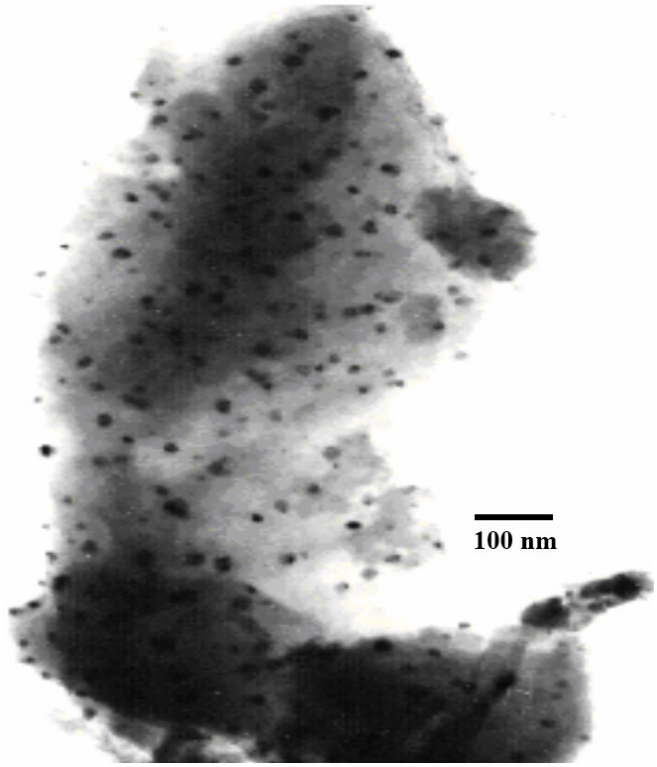

Fig. (9). TEM image of Ni-Ca/AC after 90 min reaction at 650ºC.

3.3. Summary and General Discussion

A summary of the above discussion can be pointed out. In agreement with the proposed mechanism of Baker *et al.* [26] the nickel nanoparticles are trapped (Fig. **8**) because the carbon nanotubes are growing from the particle acting as catalyst. After growth, MW-CNT can be destroyed by the applied experimental conditions, and mixtures of nickel nanoparticles plus carbon are obtained (Figs. **9**, **10**). Eventually, this carbon deposits would be *in situ* activated by CO_2, with the concomitantly increase in surface area (Table **1**). Rigorous kinetic studies of activity of Ni-based catalysts in the methane reforming and their selectivity to carbon deposits, hydrogen and syngas have been reported using electrobalance [27] and thermobalance [28]. The results obtained in the present work are in agreement with these studies because in the experimental conditions of the present work (650ºC, 1atm) carbon dioxide is able to react with the carbon deposits formed by the methane cracking reaction. In addition, strong Lewis bases as CaO or $CaCO_3$ not only can play a promoter role as have been early reported [1-4] but also clearly influence the balance of reactions involved during dry methane reforming [28] or steam/dry methane reforming [27] and therefore, the selectivity to coke and hydrogen. Therefore, present enforces are aimed to verify the influence of physicochemical properties of activated carbon and different types of promoters on changes in activity, selectivity and stability of Ni-based catalysts during dry reforming and catalytic cracking of methane.

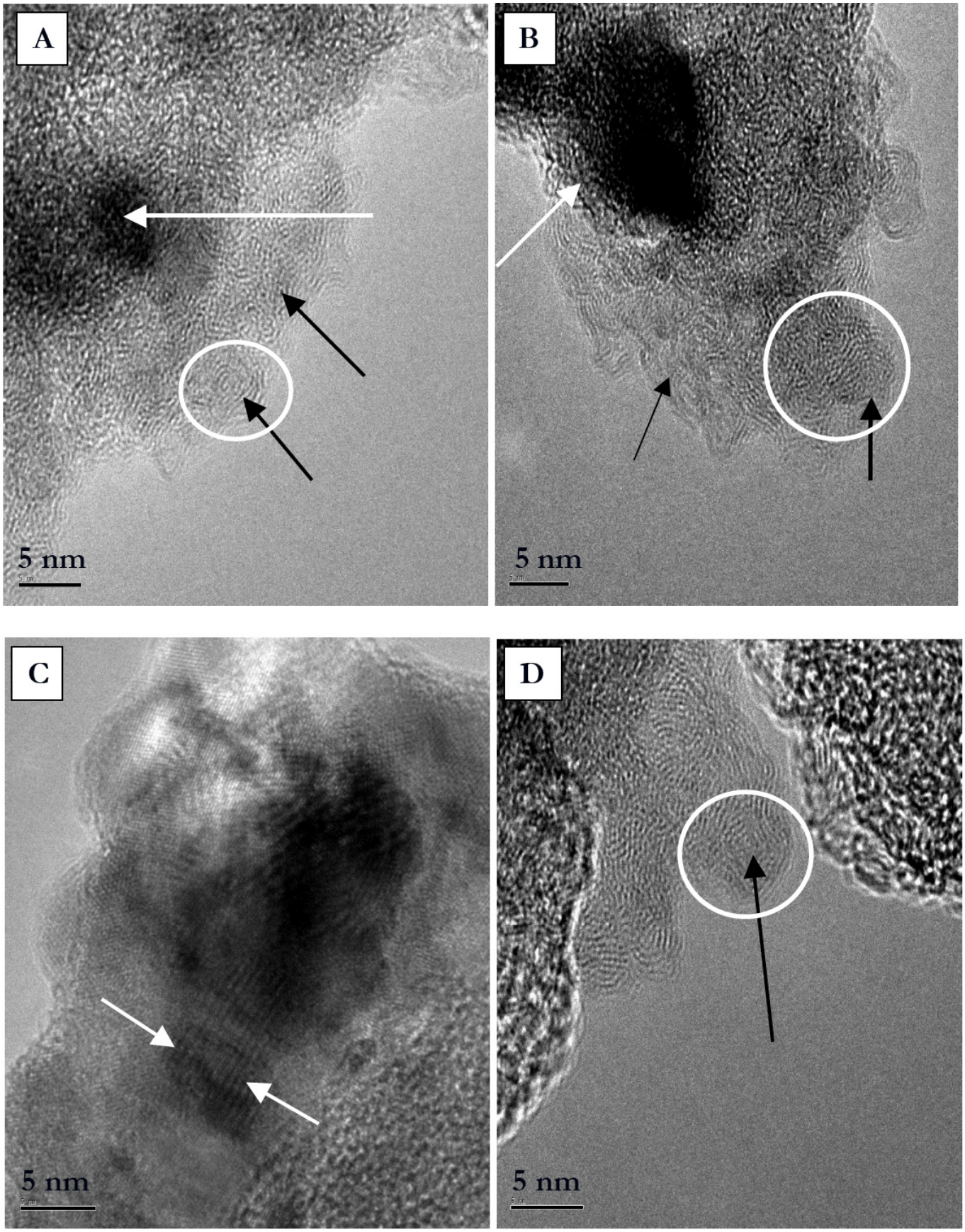

Fig. (10). HR-TEM image of Ni-Ca/AC after 90 min reaction at 650ºC. (**A**) and (**B**): Nickel nanoparticles (white arrows). (**C**): Diffusion of crystallites through several very-well aligned (white arrow) carbon layers. (**D**): Apparent morphology of carbon nano-onions (white circle).

4. CONCLUSIONS

Changes in textural properties and morphology of Ni-Ca/AC catalyst were verified during dry methane reforming. An increase in one order magnitude in surface area was detected and it was attributed to *in situ* activation by gasification with CO_2 of carbon deposits formed during reaction. HR-TEM showed diffusion of Ni nanoparticles and carbon-like nano-onions with a separation of graphene layers about 0.5nm which is consistent with the formation of a supermicroporous carbon structure. The present results suggest that introducing CO_2 pulses during reactions, carbon-supported Ni-Ca could be employed as potential catalysts for methane and other hydrocarbon reforming reactions. Our present enforces are aimed to the study of oxidation of light hydrocarbons such as ethane, propane and so on, and small organic molecules like alcohols under mild experimental conditions, mainly at low temperature and atmospheric pressure.

ACKNOWLEDGEMENTS

J. Matos thanks to Electron Microscopy Centre of Venezuelan Central University and to University of Texas for TEM and HR-TEM studies.

REFERENCES

[1] Tomishige K. Syngas production from methane reforming with CO_2/H_2O and O_2 over NiO–MgO solid solution catalyst in fluidized bed reactors. Catal Today 2004; 89: 405-18.

[2] Bradford MCJ, Vannice MA. CO_2 reforming of CH_4. Catal Rev Sci Engin 1999; 41: 1-42.

[3] Bradford MCJ, Vannice MA. Catalytic reforming of methane with carbon dioxide over nickel catalysts. Catalyst characterization and activity. Appl Catal A Gen 1996; 142: 73-96.

[4] Rostrup-Nielsen JR, Hansen JHB. CO_2 reforming of methane over transition metals. J Catal 1993; 144: 38-49.

[5] Slagterm A, Schuurman A, Leclercq C, *et al*. Specific features concerning the mechanism of methane reforming by carbon dioxide over Ni/La_2O_3 catalyst. J Catal 1997; 172: 118-26.

[6] Frusteri F, Spadaro L, Arena F, *et al*. TEM evidence for factors affecting the genesis of carbon species on bare and K-promoted Ni/MgO catalysts during the dry reforming of methane. Carbon 2002; 40: 1063-70.

[7] Bai Z, Chen H, Li B, *et al*. Methane decomposition over Ni loaded activated carbon for hydrogen production and the formation of filamentous carbon. Inter J Hydrogen Energy 2007; 32: 32-7.

[8] Matos J, Brito JL, Laine J. Activated carbon supported Ni-Mo: Effects of pretreatments and composition on catalyst reducibility and on ethylene conversion. Appl Catal A Gen 1997; 152: 27-42.

[9] Matos J, Laine J. Ethylene conversion on activated carbon supported NiMo catalysts: Effect of the support. Appl Catal A Gen 2003; 241: 25-38.

[10] Matos J, Díaz K, García V, *et al*. Methane transformation in presence of carbon dioxide on activated carbon supported nickel-calcium catalysts. Catal Lett 2006; 109: 163-9.

[11] Díaz K, García V, Matos J. Activated carbon supported Ni-Ca: Influence of reaction parameters on activity and stability of catalyst on methane reformation. Fuel 2007; 86: 1337-44.

[12] Li Y, Zhang B, Xie X, *et al*. Novel Ni catalysts for methane decomposition to hydrogen and carbon nanofibers. J Catal 2006; 238: 412-24.

[13] Li Y, Chen J, Chang L, *et al*. The doping effect of copper on the catalytic growth of carbon fibers from methane over a Ni/Al_2O_3 catalyst prepared from Feitknecht compound precursor. J Catal 1998; 178: 76-83.

[14] Harkins WD, Jura G. Surfaces of solids. XIII. A vapor adsorption method for the determination of the area of a solid without the assumption of a molecular area, and the areas occupied by Nitrogen and other molecules on the surface of a solid. J Am Chem Soc 1944; 66: 1366-73.

[15] Labib ME, Williams R. The use of zeta-potential measurements in organic solvents to determine the donor—acceptor properties of solid surfaces. J Colloids Interface Sci 1984; 97: 356-66.

[16] Kroll VCH, Delichure P, Mirodatos C. Methane reforming reaction with carbon dioxide over a Ni/SiO_2 catalyst: The nature of the active phase. Kinet Catal 1996; 37: 698-705.

[17] Resasco DE. Single Walled Carbon Nanotubes. Large-scale production and commercial applications. J Nanopart Res 2002; 4: 131-6.

[18] Wigmans T. Industrial aspects of production and use of activated carbons. Carbon 1989; 27: 13-22.

[19] Matos J, Labady M, Albornoz A, *et al*. Topological organization and textural changes of carbon macro-networks submitted to activation with N_2 and CO_2. J Mater Sci 2004; 39: 3705-16.

[20] Song Q, Xiao R, Li Y, *et al*. Catalytic carbon dioxide reforming of methane to synthesis gas over activated carbon catalyst. Ind Eng Chem Res 2008; 47: 4349-57.

[21] Ramirez S, Ferreira D, Gottberg V, *et al*. Adding a micropore framework to a parent activated carbon by carbon deposition from methane or ethylene. Carbon 2003; 41: 2653-5.

[22] Albornoz A, Labady M, López M, *et al*. Evidence for the formation of slit mesopores in activated carbon. J Mater Sci Lett 2000; 18: 1999-2000.

[23] Krasil'nikova OK, Voloshchuk AM, Evsyukhin AE, *et al*. Preparation of ultramicro-, micro-, and supermicroporous carbon adsorbents by template procedure. Colloid J 2006; 68: 182-8.

[24] Méndez MOA, Lisbôa ACL, Coutinho AR, *et al*. Activated petroleum coke for natural gas storage. J Braz Chem Soc 2006; 17: 1144-50.

[25] Imasaka K, Kanatake Y, Ohshiro Y, *et al*. Production of carbon nanoonions and nanotubes using an intermittent arc discharge in water. Thin Solid Films 2006; 506-7: 250-4.

[26] Baker RTK, Barber MA, Harris PS, *et al*. Nucleation and growth of carbon deposits from the nickel catalyzed decomposition of acetylene. J Catal 1972; 26: 51-62.

[27] Snoeck JW, Froment GF, Fowles M. Steam/CO_2 reforming of methane. Carbon Filament formation by the Boudouard reaction and gasification by CO_2, by H_2, and by steam. Ind Eng Chem Res 2002; 41: 4252-65.

[28] Gronchi P, Fumagalli D, Del Rosso R, *et al*. Carbon deposition in methane reforming with carbón dioxide. J Thermal Anal Calor 1996; 47: 227-34.

Received: September 28, 2010 Revised: November 5, 2010 Accepted: November 5, 2010

© Matos *et al.*; Licensee *Bentham Open*.

This is an open access article licensed under the terms of the Creative Commons Attribution Non-Commercial License (http://creativecommons.org/licenses/ by-nc/3.0/) which permits unrestricted, non-commercial use, distribution and reproduction in any medium, provided the work is properly cited.